by track consumption. Hence, if given the choice between two directions, these walkers can go either way. In our system, directionality is a consequence of the asymmetry of the design, which is a key component of functional Brownian motors (*4*, *5*).

Through track stem-loop consumption, our mechanism allows the walker to hybridize the fuel hairpins onto the track sequentially and dynamically according to the presence of a code on the track. Such a capability in a molecular automaton is reminiscent of the ribosome and DNA or RNA polymerase (*26*). Indeed, the leg-holding sequences are uncoupled from the fuel-grabbing sequences. Thus, in principle, a track could be encoded to hybridize with an arbitrary number of fuel molecules before the walker returned to the beginning of the fuel cycle to take further steps in the same direction. This demonstration of molecular coordination is a step toward the development of more complex and autonomous synthetic molecular motor systems, whether they are made from DNA or from other polymeric materials (*5*).

References and Notes

1. K. Svoboda *et al.*, *Nature* **365**, 721 (1993).
2. A. D. Mehta, *Nature* **400**, 590 (1999).
3. R. D. Vale, *Cell* **112**, 467 (2003).
4. R. D. Astumian, *Science* **276**, 917 (1997).
5. E. R. Kay, D. A. Leigh, F. Zerbetto, *Angew. Chem. Int. Ed.* **46**, 72 (2007).
6. W. B. Sherman, N. C. Seeman, *Nano Lett.* **4**, 1203 (2004).
7. J. S. Shin, N. A. Pierce, *J. Am. Chem. Soc.* **126**, 10834 (2004).
8. Y. Tian, Y. He, Y. Chen, P. Yin, C. Mao, *Angew. Chem. Int. Ed.* **44**, 4355 (2005).
9. R. Pei *et al.*, *J. Am. Chem. Soc.* **128**, 12693 (2006).
10. P. Yin, H. M. T. Choi, C. R. Calvert, N. A. Pierce, *Nature* **451**, 318 (2008).
11. S. J. Green, J. Bath, A. J. Turberfield, *Phys. Rev. Lett.* **101**, 238101 (2008).
12. A. J. Turberfield *et al.*, *Phys. Rev. Lett.* **90**, 118102 (2003).
13. J. S. Bois *et al.*, *Nucleic Acids Res.* **33**, 4090 (2005).
14. T. J. Fu, N. C. Seeman, *Biochemistry* **32**, 3211 (1993).
15. P. Sa-Ardyen, A. V. Vologodskii, N. C. Seeman, *Biophys. J.* **84**, 3829 (2003).
16. B. Yurke, A. J. Turberfield, J. A. P. Mills, F. C. Simmel, J. L. Neumann, *Nature* **406**, 605 (2000).
17. J. B. Mills, E. Vacano, P. J. Hagerman, *J. Mol. Biol.* **285**, 245 (1999).
18. S. B. Smith, Y. J. Cui, C. Bustamante, *Science* **271**, 795 (1996).
19. S. G. Fischer, L. S. Lerman, *Cell* **16**, 191 (1979).
20. O. Gia, S. M. Magno, A. Garbesi, F. P. Colonna, M. Palumbo, *Biochemistry* **31**, 11818 (1992).
21. Material and methods are available as supporting material on *Science* Online.
22. T. J. Fu, Y. C. Tse-Dinh, N. C. Seeman, *J. Mol. Biol.* **236**, 91 (1994).
23. A 1-hour time interval was used in all of the experiments. This was an ideal time period for handling the five radioactive track versions simultaneously because all associated denaturing and nondenaturing experiments were conducted in parallel from one stock solution (*21*). Hence, detailed results about the reaction rates of the system are not available from this study.
24. J. Mai, I. M. Sokolov, A. Blumen, *Phys. Rev. E Stat. Nonlin. Soft Matter Phys.* **64**, 011102 (2001).
25. S. Saffarian *et al.*, *Science* **306**, 108 (2004).
26. E. Shapiro, Y. Benenson, *Sci. Am.* **294**, 44 (2006).

27. We thank C. Mao, H. Yan, and N. Jonoska for critical reading of the manuscript. This research has been supported by grants to N.C.S. from the National Institute of General Medical Sciences, NSF, the Army Research Office, the Office of Naval Research, the New York Nano-Bio-Molecular Information Technology Incubator program of the Department of Energy, and the W. M. Keck Foundation.

Supporting Online Material

www.sciencemag.org/cgi/content/full/324/5923/67/DC1
Materials and Methods
SOM Text
Figs. S1 to S14
Table S1
References

29 December 2008; accepted 10 February 2009
10.1126/science.1170336

Iron-Based Catalysts with Improved Oxygen Reduction Activity in Polymer Electrolyte Fuel Cells

Michel Lefèvre,* Eric Proietti,* Frédéric Jaouen, Jean-Pol Dodelet†

Iron-based catalysts for the oxygen-reduction reaction in polymer electrolyte membrane fuel cells have been poorly competitive with platinum catalysts, in part because they have a comparatively low number of active sites per unit volume. We produced microporous carbon–supported iron-based catalysts with active sites believed to contain iron cations coordinated by pyridinic nitrogen functionalities in the interstices of graphitic sheets within the micropores. We found that the greatest increase in site density was obtained when a mixture of carbon support, phenanthroline, and ferrous acetate was ball-milled and then pyrolyzed twice, first in argon, then in ammonia. The current density of a cathode made with the best iron-based electrocatalyst reported here can equal that of a platinum-based cathode with a loading of 0.4 milligram of platinum per square centimeter at a cell voltage of ≥0.9 volt.

The desired high power density from polymer electrolyte membrane fuel cells (PEMFCs) can only be achieved by speeding up the otherwise slow reaction steps at their low operating temperatures (~80°C) through catalysis. For the oxygen-reduction reaction (ORR), non–precious metal catalysts (NPMCs), which are potentially less expensive and more abundant, have been outperformed by Pt-based catalysts (*1*, *2*), which exhibit high activity as the native metal. For metals such as Co and Fe, improved performance will require a robust method for increasing the reactivity of the metal ion through ligation.

Since 1964, when Jasinski observed that cobalt phthalocyanine catalyzed the ORR (*3*), a number of approaches have been explored to create practical NPMCs. Catalysts were first obtained by adsorbing Fe-N_4 or Co-N_4 macrocycles on a carbon support and pyrolyzing the resulting material in an inert atmosphere (*4*). A breakthrough was then achieved by Yeager when it was revealed that these often-expensive macrocycles could instead be substituted by individual N and Co precursors (*5*). This approach was followed by several groups, including ours (*4*, *6*–*16*). Meanwhile, NPMC research using metal-N_4 macrocycles has also progressed (*17*–*19*).

Our previous approach in the synthesis of NPMCs for ORR has been to use NH_3 as a nitrogen precursor. The catalysts were obtained by wet impregnation of carbon black with an iron precursor such as iron(II) acetate (FeAc), followed by a heat treatment in NH_3; we refer to the products as Fe/N/C electrocatalysts. During pyrolysis at temperatures of ≥800°C, NH_3 partly gasifies the carbon support, resulting in a mass loss that depends on the duration of the heat treatment (*20*). The disordered domains of the carbon support are preferentially gasified (*21*–*23*). As a result, micropores are created in the carbon black particles. The mass loss at which maximum activity is reached [30 to 50 weight percent (wt %)] corresponds to the largest microporous surface area for the etched carbon, which suggests that these micropores (width ≤2 nm) host most of the catalytic sites (*21*).

The reaction of NH_3 with the disordered carbon domains also produces the N-bearing functionalities needed to bind iron cations to the carbon support (*24*, *25*). It has been proposed that most of the Fe/N/C catalytic sites consist of an iron cation coordinated by four pyridinic functionalities attached to the edges of two graphitic sheets, each belonging to adjacent crystallites on either side of a slit pore in the carbon support (*21*, *25*). Thus, four factors have been identified as requirements for producing active Fe-based catalysts for ORR: (i) disordered carbon content in the catalyst precursor (*20*), (ii) iron, (iii) surface nitrogen, and (iv) micropores in the catalyst.

Our present approach, which introduces a new material (pore filler) and replaces impregnation with planetary ball-milling, has elevated the catalytic activity of an Fe-based NPMC by a factor of >35 relative to the previous best reported

Institut National de la Recherche Scientifique, Énergie, Matériaux et Télécommunication, Varennes, Québec J3X 1S2, Canada.

*These authors contributed equally to this work.
†To whom correspondence should be addressed. E-mail: dodelet@emt.inrs.ca

activity for Fe-based catalysts (*11*) (and within ~10% of the best Pt-based catalysts). Furthermore, these NPMCs may also present opportunities for ORR in direct alcohol, formic acid, and alkaline fuel cells.

For NPMCs, it is meaningful to speak in terms of volumetric activity for ORR (*1*) because its product with electrode thickness predicts the kinetic current density (A cm^{-2}) of the cathode. Because of mass-transport limitations related to electrode thickness, NPMC cathodes must attain the same kinetic current density as Pt-based cathodes without exceeding a thickness of ~100 μm (*1*). This criterion defines a target for volumetric activity (A cm^{-3}) for NPMCs. [The activity is originally measured in amperes per gram of NPMC; conversion from A g^{-1}_{NPMC} to A $cm^{-3}_{electrode}$ is described in (*26*).] For NPMCs, the U.S. Department of Energy (DOE) has set a 2010 target of 130 A cm^{-3} as measured in a fuel cell at 0.8 V *iR*-free cell voltage (i.e., after correction for ohmic loss *R*), at 80°C, and at O_2 and H_2 absolute pressures of 1 bar (*27*). All volumetric activity values reported in this work correspond to these reference conditions. For the best catalysts synthesized by our group to date by impregnation of FeAc on carbon black followed by heat treatment in NH_3 at 950°C, a volumetric activity of 0.8 to 1.5 A cm^{-3} was obtained (*28*, *29*). This value is comparable to the value of 2.7 A cm^{-3} (recalculated for O_2 and H_2 pressures of 1 bar) obtained by Wood *et al*. for a Fe/N/C catalyst (*11*). All of these activities are still well below the DOE 2010 target of 130 A cm^{-3}.

The volumetric activity is the product of the catalytic site density and the activity of a single site. The latter varies with voltage and is an intrinsic property of the catalytic site. If the catalytic activity of the site is left unchanged, increased volumetric activity can only be achieved by increasing the site density. The volumetric catalytic activity may be improved by increasing the Fe content. However, doing so increases the activity proportionally only up to

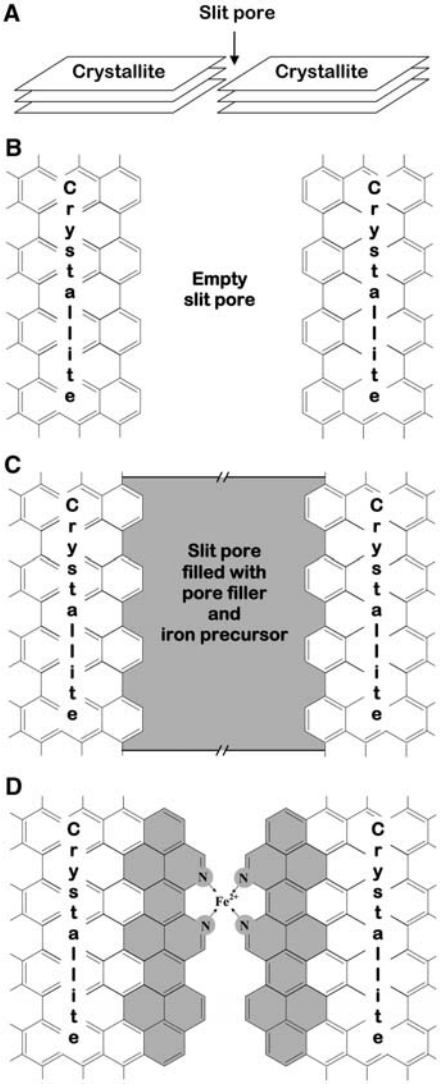

Fig. 1. Schematic representation of catalytic site formation in the micropores of the carbon support. (**A**) Simplified 3D view of a slit pore between two adjacent graphitic crystallites in the carbon support. (**B**) Plan view of an empty slit pore between two crystallites. (**C**) Plan view of a slit pore filled with pore filler and iron precursor after planetary ball-milling. (**D**) Plan view of the presumed catalytic site (incomplete) and graphitic sheet growth (shaded aromatic cycles) between two crystallites after pyrolysis.

Table 1. Catalytic activity for optimized catalysts. Volumetric activities are at 0.8 V *iR*-free cell voltage at reference conditions of 80°C and 1 bar O_2 and H_2. Black Pearls 2000 was used as the carbon support. The mass ratio of pore filler to carbon support was 1:1. Catalyst loading for all tests was ~1 mg cm^{-2}. The Nafion-to-catalyst ratio (NCR) was 2 unless otherwise noted.

Gas for first pyrolysis (1050°C)	Gas for second pyrolysis (950°C)	Pore filler	Nominal Fe content (wt %)	Catalytic activity (A cm^{-3})*
NH_3	—	PTCDA	0.2	22
NH_3	—	PTCDA	0.5	24
NH_3	—	PTCDA	1.0	30
Ar	—	Phen	0.2	2.8
Ar	—	Phen	1.0	5.5
Ar	—	Phen	4.1	1.4
Ar	NH_3	Phen	0.2	60†
Ar	NH_3	Phen	1.0	64†
Ar	NH_3	Phen	4.1	31†
Ar	NH_3	Phen	1.0	99‡ (NCR 1.5)

*Converted from the activity measured under 1.5 bar O_2 and H_2 absolute pressures to the reference pressures of 1 bar absolute pressure (*26*). †Unoptimized mass loss in second pyrolysis. ‡Optimized mass loss in first and second pyrolysis.

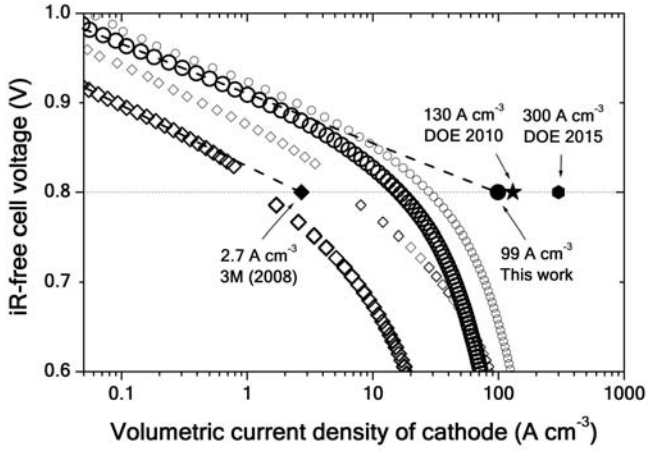

Fig. 2. Volumetric current density of best NPMC in this work. Original polarization curves were obtained from H_2-O_2 fuel cell tests at 80°C and 100% relative humidity (RH) for cathodes made with the best NPMC in this work (small open circles, P_{O_2} = P_{H_2} = 1.5 bar) and for the presumed previous best NPMC (*11*) (small open diamonds, P_{O_2} = 3.9 bar and P_{H_2} = 2.5 bar). Corrected polarization curves are based on DOE fuel cell test reference conditions (P_{O_2} = P_{H_2} = 1 bar, 80°C, 100% RH) for the best NPMC in this work (large open circles) and for the presumed previous best NPMC (*11*) (large open diamonds). A catalyst loading of ~1 mg cm^{-2} was used for all polarization curves. The actual Fe content in the catalyst from this work is 1.7 wt %, resulting in a Fe loading of 17 μg cm^{-2}. The volumetric (kinetic) current density at 0.8 V *iR*-free cell voltage for the presumed previous best NPMC (solid diamond) and the best NPMC in this work (solid circle) is the intersection of the extended Tafel slope of the corrected polarization curves (dashed lines) with the 0.8 V axis. Also included are the 2010 (star) and 2015 (hexagon) DOE performance targets for ORR on NPMCs, all at the reference conditions of P_{O_2} = P_{H_2} = 1 bar, 80°C, and 100% RH.

~0.2 nominal wt % Fe, beyond which the activity levels off and eventually decreases (*29*). Furthermore, when catalysts were prepared using he impregnation method on nonmicroporous carbon black and pyrolyzed in pure NH_3, the micropore surface area of the resulting catalysts was shown to govern the catalytic activity; the nitrogen and iron content were usually nonlimiting (*21*).

In a recent study, we impregnated FeAc onto highly microporous carbon supports followed by pyrolysis in NH_3 (*30*). An example of a highly microporous carbon black is Black Pearls 2000 with a Brunauer-Emmett-Teller (BET) surface area of 1379 $m^2\ g^{-1}$ and a micropore area of 934 $m^2\ g^{-1}$. By contrast, a typical carbon support of lower porosity such as Vulcan XC-72R has a BET surface area of 213 $m^2\ g^{-1}$ and a micropore area of 114 $m^2\ g^{-1}$. Surprisingly, the use of highly microporous carbon supports did not improve the activity relative to catalysts made with nonmicroporous carbon supports. We concluded that only the micropores created during heat treatment in NH_3 may host catalytic sites. The micropores in the as-received microporous carbon blacks do not bear the surface nitrogen necessary to form catalytic sites. Because these carbon blacks have little disordered carbon content, surface nitrogen is difficult to add during pyrolysis in NH_3.

In the present work, to capitalize on the high micropore content of microporous carbon blacks and to overcome the limitations resulting from their lack of disordered carbon, we filled these micropores with a mixture of pore filler (PF) and iron precursor (Fig. 1). Doing so created a catalyst precursor that complies with the factors required for producing active NPMCs, as described above. To overcome the limitation of solubility and/or adsorbability associated with the impregnation method, we used planetary ball-milling to fill the pores of the microporous carbon support with PF and iron precursor. Planetary ball-milling uses both friction and impact effects to force the filler materials (PF and iron precursor) into the pores of the carbon support while leaving its microstructure relatively unaffected.

For all catalysts in the present work, we used Black Pearls 2000 (Cabot; micropore surface area 934 $m^2\ g^{-1}$) as the microporous carbon black and FeAc as the iron precursor. Micropores are defined as pores having a width of ≤20 Å. We chose two pore fillers: perylene-tetracarboxylic dianhydride (PTCDA), which is nitrogen-free, and 1,10-phenanthroline (phen), which is N-bearing. For catalysts made using PTCDA, the N atoms necessary to form catalytic sites arise from its reaction with NH_3 during pyrolysis. For catalysts made with phen, the pyrolysis may be performed either in Ar or NH_3 because phen already contains nitrogen. Note that phen forms a complex with Fe^{2+}.

We first investigated the effect of the wt % of PTCDA in the catalyst precursor. Four different wt % PTCDA values (0, 25, 50, 75) were used with a constant nominal Fe loading of 0.2 wt %. Optimal volumetric activities of 1.8, 8.5, 22, and 27 A cm^{-3} were obtained, respectively. The experimental conditions and corresponding fuel cell polarization curves are given in fig. S3 (*26*). Next, a PF loading of 50 wt % (PTCDA or phen) was chosen to investigate the effect of nominal Fe loading in the catalyst precursor. Catalyst precursors made with PTCDA were pyrolyzed in NH_3 and those made with phen in Ar, both at 1050°C. Although better volumetric activities were obtained with the PTCDA series (Table 1), we investigated the effect of a subsequent 5-min pyrolysis in NH_3 for the phen series. This subsequent pyrolysis amplified the volumetric activity of the Ar-pyrolyzed phen series by a factor of ≤20. These amplified activities surpassed those of the PTCDA series. Given the notable improvement in activity of the phen-based catalysts after a second pyrolysis in NH_3, we prepared phen-based catalysts (with 1 wt % nominal Fe content) using a single pyrolysis in NH_3 at 1050°C. The volumetric activities of the latter catalysts (16 to 29 A cm^{-3}) were lower than those achieved using a two-step pyrolysis, first in Ar at 1050°C, then in NH_3 at 950°C.

Two factors were further optimized on the most active catalyst corresponding to 1 wt % nominal Fe content (64 A cm^{-3}, Table 1): (i) the mass loss during pyrolysis in NH_3, and (ii) the Nafion-to-catalyst ratio (NCR) in the cathode (Nafion is a proton-conducting perfluoro polyethylene sulfonic acid polymer made by DuPont). The optimal mass loss and NCR were found to be ~30% and ~1.5, respectively, leading to an increase in volumetric activity from 64 to 99 A cm^{-3}, which is much closer to the 2010 DOE performance target of 130 A cm^{-3} for ORR on NPMCs. (See table S2 for additional details on mass activity, mass loss during pyrolysis, micropore surface area, and nitrogen content.)

Polarization curves (both as-measured and corrected to the DOE fuel cell test reference conditions) in terms of volumetric current density for our best NPMC and for the presumed best NPMC reported to date by Wood *et al.* (*11*) are shown in Fig. 2. The DOE volumetric activity target for ORR on NPMCs is specified for 0.8 V *iR*-free cell voltage and under reference conditions. The kinetic activity (free of ohmic and mass transport losses) of the NPMCs at 0.8 V *iR*-free cell voltage cannot be directly read from the corrected polarization curves, but must instead be estimated by extrapolating the kinetically controlled Tafel slope observed at higher cell voltage. Our best NPMC shows a factor of >35 activity enhancement relative to the presumed previous best NPMC.

To compare these NPMCs for ORR in PEMFCs to precious metal catalysts, Fig. 3 shows, in terms of current density, the polarization curves of the best NPMC produced in this work (Table 1, last row) using two catalyst loadings, 1.0 and 5.3 mg cm^{-2}, compared with that of a Pt-based cathode catalyst (~0.4 mg cm^{-2} Pt) tested under the same conditions and test fuel cell. At 0.9 V *iR*-free cell voltage, where both polarization curves are within the kinetically controlled Tafel region, increasing the loading of the NPMC by a factor of ~5 increases the current density of the cell by about the same factor. At 0.9 V, the current density of the cathode with the NPMC (5.3 mg cm^{-2}) is equal to that with the Pt-based cathode. Although the NPMC loading of ~5 mg cm^{-2} is much greater than that for Pt (0.4 mg cm^{-2}), the limiting factor for the Pt loading is materials cost, unlike the low-cost NPMCs in this work (*31*). On the other hand, the limiting factor for NPMC loading is electrode thickness, which, if increased beyond ~100 μm (*1*), creates unacceptable mass transport losses at high current density, resulting in decreased power density. Indeed, Fig. 3 clearly shows how increasing the electrode thickness of the NPMC cathode raises the current density to that of the Pt-based cathode at high cell voltage,

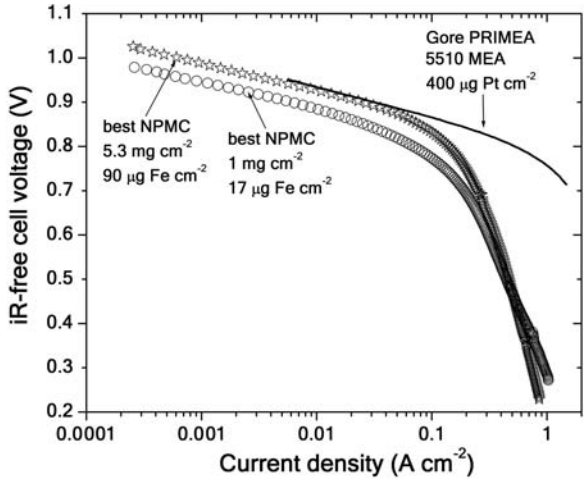

Fig. 3. Comparison of the best NPMC in this work with a Pt-based catalyst. Polarization curves from H_2-O_2 fuel cell testing ($P_{O_2} = P_{H_2}$ = 1.5 bar, 80°C, 100% RH) are shown for cathodes made with the best NPMC in this work, one with a loading of 1 mg cm^{-2} (circles) and another with a loading of 5.3 mg cm^{-2} (stars). Also shown is a ready-to-use Gore PRIMEA 5510 membrane electrode assembly (MEA; W. L. Gore & Associates) with ~0.4 mg Pt cm^{-2} at cathode and anode (black line). Flow rates for H_2 and O_2 were well above stoichiometric. The actual Fe content in our catalyst is 1.7 wt %, resulting in a Fe loading of 17 μg cm^{-2} for a catalyst loading of 1 mg cm^{-2}. Open circuit voltages are 1.03, 1.03, and 1.01 V for the MEAs using 17 and 90 μg Fe cm^{-2} and 400 μg Pt cm^{-2} at the cathode, respectively.

but creates increased mass transport losses at current densities of >0.1 A cm^{-2}. It is clear from these results that improvements in electrode mass transport properties are required to overcome this performance loss.

The results of 100-hour durability tests in fuel cells using hydrogen/oxygen and hydrogen/air as anode/cathode gases are shown in fig. S4. Relative to the stable current densities obtained by Bashyam and Zelenay (*32*) for tests performed under the same conditions (0.2 A cm^{-2} with H_2/O_2 at 0.5 V; 0.13 to 0.14 A cm^{-2} with H_2/air at 0.4 V), the initial current densities produced by the catalyst in this work (0.75 A cm^{-2} with H_2/O_2 at 0.5 V; 0.58 A cm^{-2} with H_2/air at 0.4 V) were much higher and remained higher throughout the 100-hour period, with final values of 0.33 A cm^{-2} with H_2/O_2 at 0.5 V and 0.36 A cm^{-2} with H_2/air at 0.4 V.

The best NPMC in this work has a much higher initial activity, but less stability, than those prepared by Bashyam and Zelenay according to a nonpyrolytic method based on a cobalt salt and polypyrrole deposited on carbon black (*32*). Continued research must now focus on improving the stability of these NPMCs and optimizing their cathode mass-transport properties.

References and Notes

1. H. A. Gasteiger, S. S. Kocha, B. Sompalli, F. T. Wagner, *Appl. Catal. B* **56**, 9 (2005).
2. H. A. Gasteiger, J. E. Panels, S. G. Yan, *J. Power Sources* **127**, 162 (2004).
3. R. Jasinski, *Nature* **201**, 1212 (1964).
4. J. P. Dodelet, in *N4-Macrocyclic Metal Complexes*, J. H. Zagal, F. Bedioui, J. P. Dodelet, Eds. (Springer, New York, 2006), pp. 83–147.
5. S. Gupta, D. Tryk, I. Bae, W. Aldred, E. Yeager, *J. Appl. Electrochem.* **19**, 19 (1989).
6. M. Yuasa *et al.*, *Chem. Mater.* **17**, 4278 (2005).
7. N. P. Subramanian *et al.*, *J. Power Sources* **157**, 56 (2006).
8. E. B. Easton, A. Bonakdarpour, J. R. Dahn, *Electrochem. Solid State Lett.* **9**, A463 (2006).
9. R. Z. Yang, A. Bonakdarpour, E. B. Easton, P. Stoffyn-Egli, J. R. Dahn, *J. Electrochem. Soc.* **154**, A275 (2007).
10. J. Maruyama, I. Abe, *Chem. Commun.* **2007**, 2879 (2007).
11. T. E. Wood, Z. Tan, A. K. Schmoeckel, D. O'Neill, R. Atanasoski, *J. Power Sources* **178**, 510 (2008).
12. A. Garsuch, K. MacIntyre, X. Michaud, D. A. Stevens, J. R. Dahn, *J. Electrochem. Soc.* **155**, B953 (2008).
13. T. Schilling, M. Bron, *Electrochim. Acta* **53**, 5379 (2008).
14. A. H. C. Sirk, S. A. Campbell, V. I. Birss, *J. Electrochem. Soc.* **155**, B592 (2008).
15. J. Maruyama, N. Fukui, M. Kawaguchi, I. Abe, *J. Power Sources* **182**, 489 (2008).
16. V. Nallathambi, J.-W. Lee, S. P. Kumaraguru, G. Wu, B. N. Popov, *J. Power Sources* **183**, 34 (2008).
17. U. I. Koslowski, I. Abs-Wurmbach, S. Fiechter, P. Bogdanoff, *J. Phys. Chem. C* **112**, 15356 (2008).
18. J. Maruyama, J. Okamura, K. Miyazaki, Y. Uchimoto, I. Abe, *J. Phys. Chem. C* **112**, 2784 (2008).
19. J. M. Ziegelbauer *et al.*, *J. Phys. Chem. C* **112**, 8839 (2008).
20. F. Jaouen, F. Charreteur, J. P. Dodelet, *J. Electrochem. Soc.* **153**, A689 (2006).
21. F. Jaouen, M. Lefèvre, J. P. Dodelet, M. Cai, *J. Phys. Chem. B* **110**, 5553 (2006).
22. F. Jaouen, J. P. Dodelet, *J. Phys. Chem. C* **111**, 5963 (2007).
23. F. Jaouen, A. M. Serventi, M. Lefevre, J. P. Dodelet, P. Bertrand, *J. Phys. Chem. C* **111**, 5971 (2007).
24. F. Jaouen, S. Marcotte, J. P. Dodelet, G. Lindbergh, *J. Phys. Chem. B* **107**, 1376 (2003).
25. F. Charreteur, F. Jaouen, S. Ruggeri, J. P. Dodelet, *Electrochim. Acta* **53**, 2925 (2008).
26. See supporting material on *Science* Online.
27. U. S. Department of Energy, Technical Plan: Fuel Cells, 2007 (www1.eere.energy.gov/hydrogenandfuelcells/mypp/pdfs/fuel_cells.pdf).
28. F. Charreteur, S. Ruggeri, F. Jaouen, J. P. Dodelet, *Electrochim. Acta* **53**, 6881 (2008).
29. F. Jaouen, J. P. Dodelet, *Electrochim. Acta* **52**, 5975 (2007).
30. M. Lefèvre, J.-P. Dodelet, *Electrochim. Acta* **53**, 8269 (2008).
31. Although detailed cost analysis of these Fe-based electrocatalysts was not performed, their principal elements are carbon, nitrogen, and iron and they require no expensive precursors or processing steps. Their manufacturing cost is conservatively estimated to be at least two orders of magnitude lower than that of current Pt-based ORR catalysts for PEMFCs.
32. R. Bashyam, P. Zelenay, *Nature* **443**, 63 (2006).

33. Supported by General Motors of Canada and the Natural Sciences and Engineering Council of Canada. The Cabot Corporation provided the carbon black. U.S. patent application US 61/112,844 related to this work was filed on 10 November 2008.

Supporting Online Material

www.sciencemag.org/cgi/content/full/324/5923/71/DC1
Materials and Methods
SOM Text
Figs. S1 to S4
Tables S1 and S2
References

19 December 2008; accepted 9 February 2009
10.1126/science.1170051

Consecutive Thermal H_2 and Light-Induced O_2 Evolution from Water Promoted by a Metal Complex

Stephan W. Kohl,[1] Lev Weiner,[2] Leonid Schwartsburd,[1] Leonid Konstantinovski,[2] Linda J. W. Shimon,[2] Yehoshoa Ben-David,[1] Mark A. Iron,[2] David Milstein[1]*

Discovery of an efficient artificial catalyst for the sunlight-driven splitting of water into dioxygen and dihydrogen is a major goal of renewable energy research. We describe a solution-phase reaction scheme that leads to the stoichiometric liberation of dihydrogen and dioxygen in consecutive thermal- and light-driven steps mediated by mononuclear, well-defined ruthenium complexes. The initial reaction of water at 25°C with a dearomatized ruthenium (II) [Ru(II)] pincer complex yields a monomeric aromatic Ru(II) hydrido-hydroxo complex that, on further reaction with water at 100°C, releases H_2 and forms a cis dihydroxo complex. Irradiation of this complex in the 320-to-420–nanometer range liberates oxygen and regenerates the starting hydrido-hydroxo Ru(II) complex, probably by elimination of hydrogen peroxide, which rapidly disproportionates. Isotopic labeling experiments with $H_2{}^{17}O$ and $H_2{}^{18}O$ show unequivocally that the process of oxygen–oxygen bond formation is intramolecular, establishing a previously elusive fundamental step toward dioxygen-generating homogeneous catalysis.

The design of efficient catalytic systems for splitting water into H_2 and O_2, driven by sunlight without the use of sacrificial reductants or oxidants, is among the most important challenges facing science today, underpinning the long-term potential of hydrogen as a clean, sustainable fuel (*1*, *2*). In this context, it is essential to enhance our basic understanding of the fundamental chemical steps involved in such processes (*3*–*17*). Of the two parts of the water-splitting cycle, the oxidation half-cycle to form O_2 presents the greatest challenge. Well-defined metal complexes that catalyze water oxidation to dioxygen are rare and generally require a sacrificial strong oxidant. The molecular mechanisms of such systems, including that of the intensively studied "blue dimer" *cis*,*cis*-$[(bpy)_2(H_2O)Ru^{III}ORu^{III}(OH_2)(bpy)_2]^{4+}$ (*3*, *11*, *12*), are generally thought to involve metal oxo intermediates and bimolecular steps, but clarification of the fundamental chemical principles responsible for O–O bond formation remains a considerable challenge. In addition, a major challenge faced by hydrogen and oxygen photogeneration systems based on soluble metal complexes is that for a viable system, the two half-cycles must be combined, avoiding the use of sacrificial oxidants and reductants. We present here a ruthenium-mediated reaction sequence that, in a stepwise stoichiometric manner, generates hydrogen thermally and oxygen photochemically, involves well-defined complexes, and demonstrates the feasibility of unimolecular O–O bond formation at a single metal center.

[1]Department of Organic Chemistry, The Weizmann Institute of Science, Rehovot 76100, Israel. [2]Department of Chemical Research Support, The Weizmann Institute of Science, Rehovot 76100, Israel.

*To whom correspondence should be addressed. E-mail: david.milstein@weizmann.ac.il

Iron-Based Catalysts with Improved Oxygen Reduction Activity in Polymer Electrolyte Fuel Cells

Michel Lefèvre, Eric Proietti, Frédéric Jaouen and Jean-Pol Dodelet

Science **324** (5923), 71-74.
DOI: 10.1126/science.1170051